Physics of the Earth and Planetary Interiors, 54 (1989) 64–81
Elsevier Science Publishers B.V., Amsterdam – Printed in The Netherlands

The core shadow zone boundary and lateral variations of the P velocity structure of the lowermost mantle

Christopher J. Young and Thorne Lay

Department of Geological Sciences, University of Michigan, Ann Arbor, MI 48109 (U.S.A.)

Young, C.J. and Lay, T., 1989. The core shadow zone boundary and lateral variations of the P velocity structure of the lowermost mantle. Phys. Earth Planet. Inter., 54: 64–81.

The recent determination of high-quality, short-period P-wave amplitude profiles near the core shadow zone for three source–receiver combinations allows an exploration of lateral variations in P velocity structure at the base of the mantle. Various radially symmetric models are tested by comparison of the data with amplitudes measured from generalized ray theory synthetics. The assumption necessary to justify one-dimensional modeling—that each of the profiles is most sensitive to scales of heterogeneity larger than the discrete regions sampled—is well supported by the coherence of the individual profiles. The observed amplitude versus distance profiles exhibit significant regional variations of the apparent shadow zone boundary, with as much as a 5° shift in onset distance, but it is possible to model the overall behavior using simple, regionally varying, positive P velocity gradients in the lowermost mantle. Velocity models with pervasive negative velocity gradients in the D″ layer are not consistent with the data. The modeling indicates that D″ velocities beneath the North Pole are ~ 2% slower than those beneath the central Pacific, while velocities beneath the North Pacific are ~ 1% faster. Although the simplest class of successful models begins to deviate from the PREM reference Earth model as much as 690 km above the core–mantle boundary, these models do not violate global mantle velocity constraints, and the theoretical slowness values calculated for the three models are consistent with slowness measurements for the same general regions. More complex, multiple-gradient lower mantle velocity structures with a thinner zone of lateral heterogeneity may be compatible with the P wave data, but such detailed structures cannot be resolved by our modeling (though bounds can be placed on viable structures). The strong lateral variations required by the data support the presence of compositional heterogeneity in D″, and the data require that at least in several locations the predominant P velocity gradients in D″ are positive.

1. Introduction

For a radially symmetric Earth model, geometric ray theory predicts that a decrease of the velocity gradient to sub-critical (i.e., $dv/dr < v/r$) will produce a gap in the travel time curve, and, consequently, a sudden drop in amplitude with distance. This is because rays cannot turn at depths having sub-critical gradients, so there will be a range of distances where there are no geometric arrivals. The foremost example of this effect in the Earth is the core shadow zone, which is caused by the abrupt decrease in seismic velocity at the core–mantle boundary (hereafter: CMB). Geometric ray theory does not, however, adequately predict the effects of the low-velocity core on body wave amplitudes because it does not account for diffraction or finite frequency effects. Diffracted arrivals are observed throughout the shadow zone, and the finite frequencies of waves bottoming just above the CMB are sensitive to the low-velocity core, resulting in a frequency-dependent decrease in amplitude before the actual onset of the geometric shadow zone. This sensitivity can be exploited to determine the velocity structure near the CMB.

The basic nature of the core shadow zone has been understood for some time, but recent improvements in seismic modeling techniques, particularly for long-period body waves (e.g., Chapman and Phinney, 1972; Doornbos and Mondt, 1979; Mula and Müller, 1980; Doornbos, 1983), have made it possible to investigate the more subtle features of core diffraction and its dependence on the velocity structure of the lowermost mantle and outermost core. Simple models, with

0031-9201/89/$03.50

variable positive or negative velocity gradients above the CMB, have been produced by these long-period studies, but there is no agreement on a single best model. Given the greater resolution of short-period P-wave signals, detailed modeling of such data would seem to have clear advantages over long-period modeling for determining the velocity structure near the CMB; however, the first-order complications due to source and propagation effects limit the resolution of most short-period analyses.

Ruff and Helmberger (1982), using a data set of short-period P-wave amplitudes from Soviet nuclear tests recorded at Worldwide Standardized Seismograph Network (WWSSN) stations in North America, obtained a four-fold reduction of amplitude scatter by applying the station corrections of Butler and Ruff (1980). The resulting data set was used to model the P velocity structure above the CMB beneath the North Pole. Ruff and Helmberger (1982) demonstrated that significant features in short-period P-wave amplitude versus distance curves, including shifts of the shadow boundary of several degrees, can be produced by varying the velocities in the lowermost few hundred kilometers of the mantle (the D″ region). They identified a general class of lower mantle velocity models that satisfied their data set (the POLAR models), which have in common a strong reduction in velocity gradient in the lower mantle about 200 km above the CMB, followed by a relatively strong positive velocity gradient extending down to the CMB. The latter feature is particularly significant, since most recent seismic analyses have indicated the presence of weak or negative velocity gradients in D″ (Doornbos, 1983; Young and Lay, 1987a). Ruff and Helmberger suggested that their data set could be globally representative, and proposed interpretations of the POLAR models with major implications for the thermal structure near the CMB. However, the D″ region is known to be heterogeneous (see Young and Lay (1987b) for a review), and a recent study of short-period P-wave amplitude data for two other D″ regions (Ruff and Lettvin, 1984), which employed the same methodology of applying receiver corrections to reduce the scatter in amplitude versus distance profiles, established that there is no single, globally representative, short-period P-wave amplitude profile: data profiles for different source–receiver combinations are coherent but unquestionably different. This variation in P-wave amplitude behavior near the core-shadow onset offers a valuable means for exploring the lateral heterogeneity of D″.

A great deal of attention has been focused on determining the velocity structure of the lowermost mantle because it is likely that this region plays a significant role in mantle convection. Estimates of the heat flux out of the molten outer core indicate that there should be a thermal boundary layer at the base of the mantle (Jeanloz and Richter, 1979; Stacey and Loper, 1983). Such a hot thermal boundary layer will have low viscosity and may serve as a source of ascending plumes, some of which may penetrate into the upper mantle (Loper and Stacey, 1983; Stacey and Loper, 1983). The base of the mantle may also represent a catchment for cold subducted material from the upper mantle (Hofmann and White, 1982). The tremendous density contrast across the CMB makes it a likely place for a chemical boundary layer to form (e.g., Ruff and Anderson, 1980), perhaps by differentiation processes similar to those which formed the lithospheric compositional boundary layer at the surface of the Earth (Jordan, 1979). Clearly, high-resolution mapping of the lowermost mantle could significantly contribute to our understanding of the dynamics of the mantle convective system.

In this paper, we demonstrate some basic relationships between simple lower mantle velocity structures and short-period P-wave amplitudes near the core-shadow zone, and then model the short-period P-wave amplitude data for the three regions studied by Ruff and Helmberger (1982) and Ruff and Lettvin (1984). The implications of the resulting laterally varying P velocity models are then considered.

2. Data

The data used in this study consist of the corrected values of short period (~ 1 s) P-wave amplitudes recorded at North American WWSSN

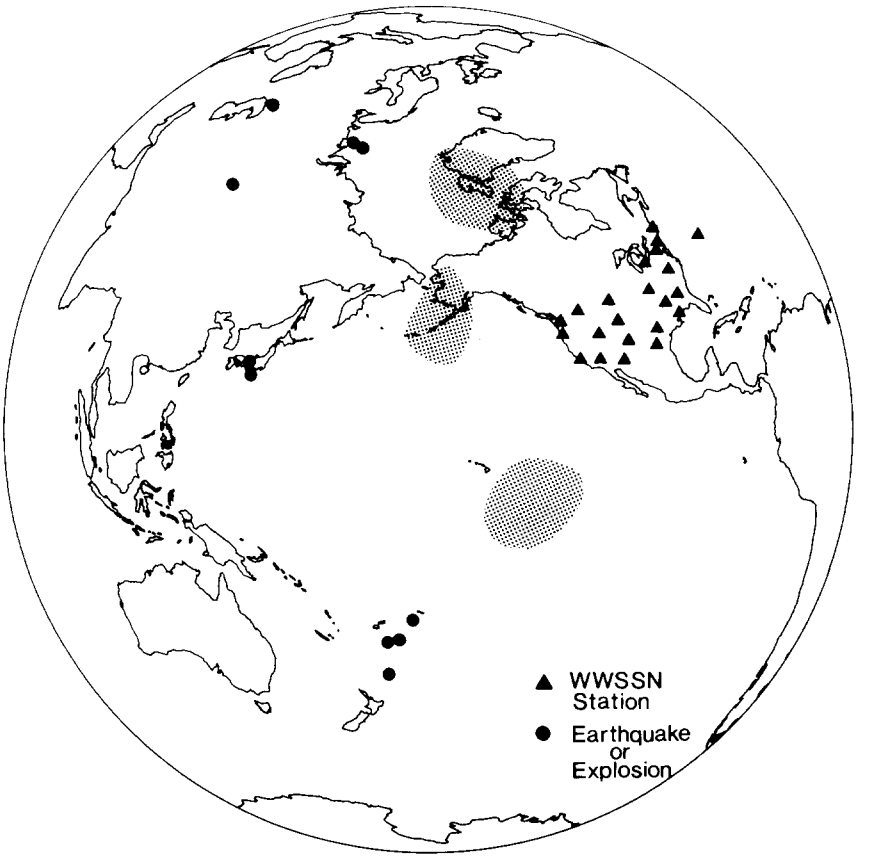

Fig. 1. An azimuthal equal area projection showing (stippled) the regions of D″ sampled by data modeled in this study. Also shown are the locations of the sources (earthquakes and explosions) and the WWSSN North American stations at which the data were recorded.

stations for Soviet nuclear tests (Ruff and Helmberger, 1982), and for earthquakes in Tonga and Japan (Ruff and Lettvin, 1984). The amplitude corrections for depth effects and receiver characteristics are described in the former paper. An additional correction for focal mechanism was applied to the earthquake data (Ruff and Lettvin, 1984). The Soviet test data sample the lower mantle beneath the North Pole region, the Japan earthquake data sample beneath the North Pacific, and the Tonga earthquake data sample beneath the Central Pacific (Fig. 1).

Since all the data have been corrected to a common surface focus, the profiles for the three regions can be directly compared (Fig. 2). All three data sets have nearly constant amplitudes out to the onset of the core shadow zone, which is at $\sim 90°$ for the North and Central Pacific data and $\sim 95°$ for the North Pole data. The amplitudes for each profile have been shifted by a constant factor so that the constant amplitude portions lie on a common baseline. This is valid because only the relative amplitudes within each profile are significant. The decay slopes in the shadow zones are ~ -0.7 for the Central Pacific, ~ -0.9 for the North Pacific, and ~ -1.3 for the North Pole, all in units of $\log_{10}\text{Amp}/10°$. While there is substantial scatter in the basic data set, we are confident that the regional differences indicated by the patterns in Fig. 2 can be resolved and warrant modeling to account for the variability. We begin by considering the general amplitude

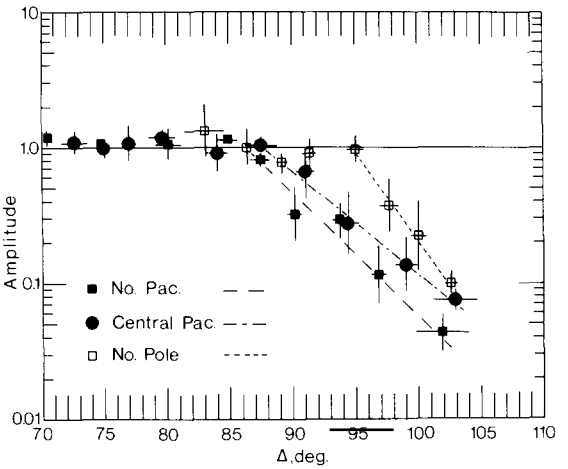

Fig. 2. A log amplitude versus distance summary plot of all of the short-period P-wave amplitude data used in this study. Each symbol represents an average of several data points: the horizontal bar indicates the range of distances spanned by the averaged data, the vertical bar is an error bound.

effects expected for various radial, deep mantle models.

3. Lower mantle velocity structure and short-period amplitude decay

The geometric shadow zone boundary is defined by the arrival distance of the geometric ray that just grazes the CMB. Any rays with smaller take-off angles will either reflect off the core (PcP), or enter the core (e.g., PKP, PKKP, etc.). The short-period P-wave amplitudes should drop drastically beyond the shadow boundary, since diffraction causes very rapid attenuation of short-period energy. The primary cause for the decrease of amplitude in the core shadow zone is the refraction of energy into the low-velocity core, but we must also consider the interference of the P and PcP arrivals.

PcP is a very small phase at distances $> 70°$ owing to its rapid geometric spreading and low reflection coefficient, so it is perhaps surprising that the phase has any effect on the P-wave amplitude at all. However, the reflection coefficient for PcP, which is positive and small at 70°, becomes negative at $\sim 85°$. At greater distances it becomes increasingly negative and the PcP–P differential time decreases, so PcP interferes destructively with P, leading to a decrease in the overall P-wave amplitude. This interference is not obvious because PcP becomes large enough to be seen only after its time separation from direct P is so small that the PcP arrival is obscured by the short-period instrument response to direct P. While the reduction in amplitude caused by the interference is measurable, our modeling indicated that it is relatively minor in comparison with the much greater decrease in amplitude owing to the refraction of energy into the core.

The detailed velocity structure of the lowermost mantle has a strong effect on many of the characteristics of the shadow zone, including its onset distance, sharpness, and the slope of the amplitude decay within it (Ruff and Helmberger, 1982). To quantify this effect, we calculated synthetic short-period P-wave waveforms for several different types of lower mantle velocity models using the generalized ray technique (see, e.g., Helmberger, 1974) and measured amplitudes directly from the synthetics. Ruff and Helmberger (1982) used both the generalized ray and full wave methods to calculate synthetic seismograms, and found that, as long as the medium has smooth velocity gradients, the generalized ray method produces reliable synthetics, even at moderate distances into the shadow zone.

All of the models which we explored are modifications of the reference radial Earth model PREM (Dziewonski and Anderson, 1981). The PREM velocity gradient in the lower mantle is a nearly constant 0.12 km s^{-1} per 100 km to a depth of 150 km above the CMB, where it abruptly decreases to 0.02 km^{-1} s per 100 km. For our initial modeling, we chose to extend the former gradient to a given depth, 690, 150, or 75 km above the CMB, and then form several models for each depth, with different constant velocity gradients extending down to the CMB. We consider these two-gradient models to be the 'simplest' class of velocity models, in terms of their parametric description. The 75- and 150-km cases were chosen because these are typical thicknesses proposed for CMB boundary layers (e.g., Doornbos and Mondt, 1979), although Anderson (1987) has

recently argued that the thermal boundary layer at the base of the mantle may be significantly thicker. The 690-km (2200 km deep) models were included to investigate the effects of relaxing the constraint of limiting gradient changes to the D″ region, which is generally identified as the lowermost 200–300 km of the mantle.

As the data profiles have already been corrected for source radiation patterns, it was not necessary to include focal mechanisms in our calculations of the synthetics. A simple step displacement was used as the source, and a t^* of 1.5 s was used to match the basic frequency content of the observations. First peak to first trough amplitudes were measured for the synthetics (the data amplitudes were measured either as first peak to first trough or as first trough to second peak, dependent on which was more distinct), and baseline amplitude shifts for plots of log amplitude versus distance were determined by averaging amplitude values for distances closer than the shadow zone boundary.

Let us consider the 690-km models first: 690.B, 690.C, and 690.D (Fig. 3a). Along with this set of models we included Model 690.A, which does not have a change in velocity gradient (i.e., it is PREM without a decreased gradient in the D″ layer). This is an important model to include for isolating the effects of varying the lower mantle velocity gradient. The log amplitude versus distance curve for 690.A is very simple, showing a nearly constant amplitude out to a distance of 90°, where the amplitudes quite abruptly begin to decrease at a rate of $\sim -1.2 \log_{10}\text{Amp}/10°$. Note that this simple behavior would, in fact, match any of the observed data sets in Fig. 2 quite well if the entire curve could be shifted along the distance axis. The way to produce such a shift is straightforward: simply change the velocity gradient, and hence, the average velocity in the lowermost mantle. Increasing the velocity gradient above the CMB moves the shadow zone closer, while decreasing it moves the shadow zone further away. Models 690.B, 690.C, and 690.D represent such modifications: 690.B has a constant velocity gradient below 690 km which yields a velocity 1% greater at the CMB than that of 690.A, and similarly 690.C and 690.D have gradients which yield CMB

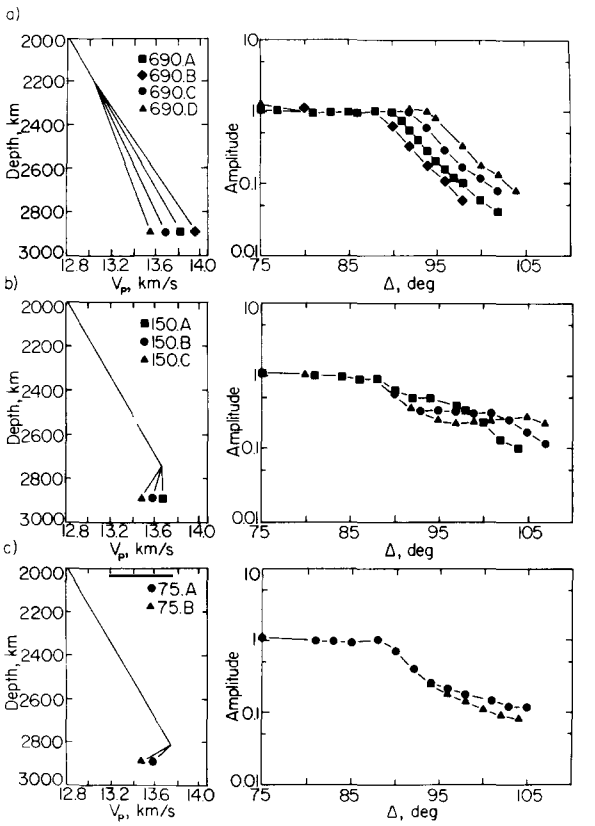

Fig. 3. A comparison of several different types of lower mantle velocity structures with the resultant short-period P-wave amplitudes generated using the generalized ray technique. (a) Models with a velocity gradient change 690 km above the CMB. (b) Models with a velocity gradient decrease 150 km above the CMB. (c) Models with a velocity gradient decrease 75 km above the CMB.

velocities 1% less than and 2% less than that of 690.A. Clearly, the resulting amplitude versus distance curves represent simple shifts along the distance axis of the curve for model 690.A, indicating that it is the average velocity in D″ which controls the distance to the shadow onset. Each of the 690 models shows the same constant amplitude behavior out to a distance beyond which there is a sharp transition to a linear log amplitude decrease. The edge of the core shadow zone is located at 88° for 690.B, 92° for 690.C and 94° for 690.D. A geometric ray turning 690 km above the CMB for any of these models will arrive at a distance of

78°, which is well within the constant amplitude portion of each of the curves, indicating that the gradient changes for these models are too subtle to produce obvious amplitude effects for rays turning near the depth of the changes. As we demonstrate in the next section, this class of very simple models is adequate for modeling the observed short-period amplitude data for all three regions.

If we only allow negative velocity gradients and confine them to the D″ region, then the results are rather more complicated. Let us first consider the case of decreases in gradient occurring at a depth of 150 km above the CMB. We computed synthetic amplitudes for three models of this type: model 150.A has a linear gradient that yields a velocity of 13.7 km s^{-1} at the CMB, and models 150.B and 150.C have gradients which yield velocities of 13.6 and 13.5 km s^{-1} respectively (Fig. 3b). By comparison, PREM has a CMB velocity of 13.72 km s^{-1}, so 150.A is nearly equivalent. The amplitude versus distance curves for these models are very different from those for the 690 models because the velocity gradient decreases are much more severe. Each curve has nearly constant amplitudes out to a distance of about 88°, where the curves begin to decrease along diverging paths. The curve for model 150.A briefly levels out between 92 and 94° and then continues to decrease. The curves for models 150.B and 150.C show similar but longer intervals of constant amplitude, 92–101° and 94–105° respectively, and then also continue to decrease.

In each case, the second amplitude decrease is the true core shadow zone, while the first decrease is caused by the reduced velocity gradient 150 km above the CMB. We explain the first decrease as follows. The velocity gradient reduction will cause a ray which would have turned at a given depth and arrived at a given distance to instead turn deeper and arrive further away. Rays which turn above the depth at which the gradient is changed are unaffected. Thus, the arrival distance difference between two rays, one turning below the changed gradient and one above, must increase while the energy transmitted within the raypaths will be fixed. The same energy is delivered over a larger area yielding lower amplitudes in the interval.

The constant amplitude intervals of the 150 profiles just before the true shadow zone onsets simply represent rays turning between the depth of the gradient change (150 km above the CMB) and the CMB, just as the constant amplitude baselines at distances $< 88°$ represent rays turning throughout the lower mantle down to the depth of the gradient change. As one would expect, the length of each interval is proportional to the severity of the velocity gradient decrease for the model.

As a limiting case, we also considered two models which have velocity gradient decreases beginning only 75 km above the CMB. These models, 75.A and 75.B (shown in Fig. 3c), reach the same CMB velocities as models 150.B and 150.C but, owing to the deeper point of gradient change, their associated decreases in velocity gradient are much greater. Model 75.A has a linear gradient of -0.25 km s^{-1} per 100 km, and model 75.B has a linear gradient of -0.39 km s^{-1} per 100 km. The critical velocity gradient at this depth is also -0.39 km s^{-1} per 100 km, so the gradient in model 75.B is actually critical. The amplitude versus distance curves for models 75.A and 75.B show amplitude decreases at 88° which are similar to those of the 150 models, but the decreases for the 75 models are somewhat stronger owing to the greater severity of the gradient change. It is not clear whether the curves for the 75 models ever level out to constant amplitudes as was the case for the 150 curves. The decay slopes do become more horizontal near 94°, but the generalized ray technique which we used does not adequately model waves very far into the shadow zone, so we did not calculate synthesis for distances beyond 105°. Nonetheless, it is clear that introducing a thin low-velocity zone at the base of the mantle will lead to a flattening of the slope of the amplitude versus distance curve in the shadow zone (compare with 690.A). Thus, the velocity gradient in D″ primarily controls the shape of the amplitude profile. Referring to the data profiles in Fig. 2, it is clear that models with strong velocity gradient

reductions will have difficulties explaining the observed amplitude decay in the shadow zone.

4. Modeling of the data

The three data sets in Fig. 2 indicate that the P wave velocity of the lowermost mantle varies laterally, which is consistent with many observations (e.g., Julian and Sengupta, 1973; Dziewonski, 1984; Woodhouse et al., 1987). On the basis of this, one could argue that modeling the data using one-dimensional velocity models like those explored in the previous section is invalid. Obviously, we must assume that the scale of heterogeneity which we are modeling is larger than the regions sampled by the data, or we cannot justifiably use a one-dimensional modeling technique. It is not possible to determine conclusively the heterogeneity spectrum within each region from our data, but the stability of the trends exhibited by each data set and the systematic differences between the data sets suggest that the profiles are primarily sensitive to a heterogeneity scale that is larger than any of the regions sampled ($\sim$ 1000 km) but smaller than the distance between them. The distance between the two closest regions, $\sim$ 2500 km, thus provides an upper bound on the scale length for which our models are valid.

There is good evidence for lateral heterogeneity in D″ on scales $\ll$ 1000 km (Doornbos and Vlaar, 1973; Sacks et al., 1979; Haddon, 1982), and it is reasonable to expect that short-period amplitude data is influenced by this small-scale heterogeneity (in fact this probably accounts for much of the scatter in the data); however, we have neither adequate data resolution nor analytic techniques to resolve deterministically the small-scale heterogeneity. Thus, we chose to model only the most robust features of the amplitude profiles: the nearly constant amplitudes prior to the onset of decay, the distance of the onset of decay, and the decay slope in the shadow zone. Our guiding philosophy is to seek the simplest model consistent with these features and to quantify those aspects of the deep mantle structure which are responsible for each feature. In their modeling of the North Pole data, Ruff and Helmberger (1982) concluded that there is a resolvable decrease in amplitude between 87 and 90°, and this feature, combined with a constraint of model perturbations to the lowest 200 km of the mantle, led to the multiple gradient complexity that all of the POLAR models show. As it is not clear that the

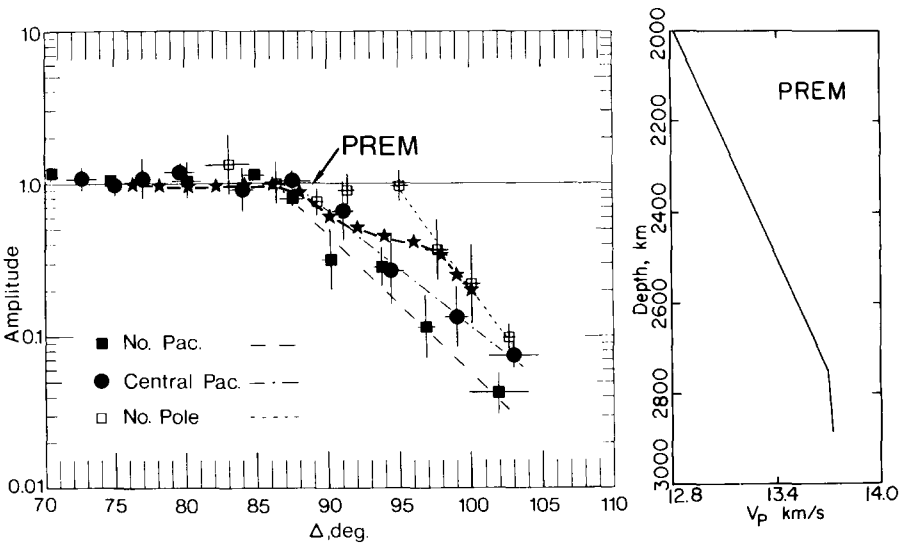

Fig. 4. (right) P-wave velocity versus depth for the PREM reference Earth model. (left) The summary plot from Fig. 2 with superimposed synthetic amplitudes (shown as stars) for the PREM model, which were calculated using the generalized ray method.

short-period amplitude data are of sufficiently high resolution to model such small amplitude fluctuations, we chose to treat the amplitudes at distances closer than the edge of the shadow zone as constant for all three data sets. We will first show the fit of synthetic amplitudes calculated for PREM to the three data sets, and then show how each data set can be fit with a different simple, locally stratified, lower mantle velocity structure.

Figure 4 shows the short-period P-wave velocity profile calculated for PREM superimposed on the summary plot of the short-period amplitude data for all three regions. In later figures where the data sets are shown individually, all of the observations for each region are plotted. Clearly, the PREM model provides a reasonable gross average behavior, but does not adequately fit any of the individual data sets. The PREM amplitudes match the constant amplitude portion of all of the data profiles, but do not match the amplitude decay portions of any of the curves. The edge of the shadow zone distance for PREM is quite similar to those of the North and South Pacific data sets, but the PREM amplitudes level out briefly between 92 and 95°, while the amplitudes of the Pacific data simply show a steady decrease. Ruff and Helmberger (1982) showed that adding a low Q region at the base of D″ does not improve the fit of a reference Earth model like PREM, so we will concentrate on more important factors: the velocity gradient and the average velocity of D″.

Comparing Fig. 4 with Fig. 3, it is clear that all three data sets can be fit best by 690-type models. The edge of the shadow zone for the Central Pacific data is at 90° similar to model 690.A, which has a constant gradient all the way to the core. The fit between data and synthetics amplitudes for this model is quite good (Fig. 5). We will henceforth refer to model 690.A as PAC0 for convenience. The synthetic amplitudes for PAC0 have constant amplitude out to 90° where they begin to decrease rapidly, in agreement with the Central Pacific data. Although the fit of the simple model PAC0 to the Central Pacific data may seem surprising, it is easily explained: the basic features of the core shadow zone—the onset distance and the decay slope in the shadow—are controlled predominantly by the average velocity and velocity gradient in D″. A simple, sharply defined shadow zone onset near 90° does not require a change of the positive velocity gradient in the lowermost mantle.

The North Pole data set is obviously different from either Pacific data set in that it has an onset of decay at ~95°, about 5° further away. Referring to Fig. 3a, it is apparent that model 690.D is

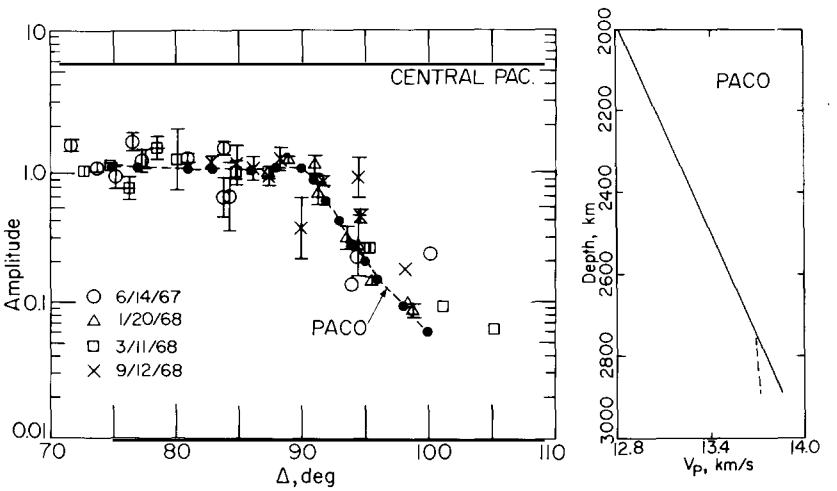

Fig. 5. Similar to Fig. 4. (right) P-wave velocity versus depth for PAC0 (model 690.A), which is shown as a solid line. The dashed line is PREM. (left) A comparison of the data for the Central Pacific D″ region with the synthetic amplitudes calculated for PAC0. The vertical bars on the data points are error bounds.

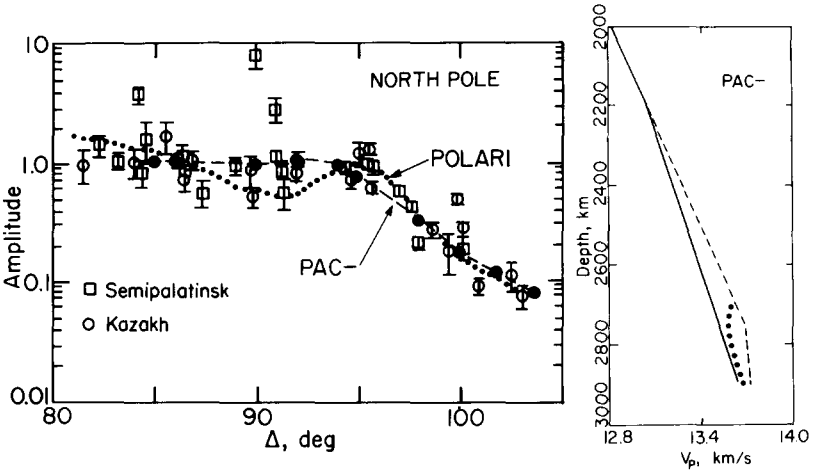

Fig. 6. As in Fig. 5, illustrating the fit of the synthetics for model PAC− (model 690.D) to the North Polar data set. The dotted line in the left figure is the profile for the POLAR1 model of Ruff and Helmberger (1982). Both models are shown in the right figure (POLAR1 is again the dotted line), along with PREM (dashed line).

quite suitable. Figure 6 shows the fit of the 690.D synthetics to the Polar data. We will hereafter refer to this model as PAC −, to indicate that it is slower than PAC0. The visual match of the synthetics and data is as good as that of the more complex POLAR models of Ruff and Helmberger (1982), which were developed to fit finer-scale features in the amplitude distance profile at distances closer than the shadow zone boundary, features which we did not feel we could resolve. One of the Ruff and Helmberger models (POLAR1) is indicated in Fig. 6. Note that POLAR1 has two features in common with PAC0: it is significantly slower than PREM within the D″ region, and has a similar positive velocity gradient in the lowermost 100 km of D″.

The North Pacific data require a slightly more complex model. This data profile has the closest onset of decay (~ 87°), so we attempted to match it with an increased velocity gradient. The basic

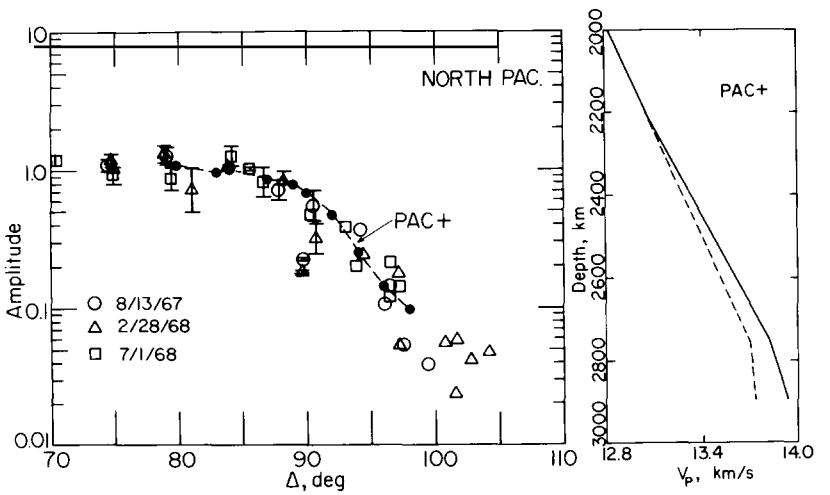

Fig. 7. As in Fig. 5, illustrating the fit of the synthetics for model PAC+ to the North Pacific data set. In the right figure, the dashed line is PREM.

character of the profile can be fit with 690.B (Fig. 3a), but this model does not fit the initial range of slight amplitude decay before the stronger decay onset at 90° (see Fig. 2). As previously shown (Fig. 3b,c), it is possible to produce such a double decay slope behavior by decreasing the gradient in D″ (though not as strongly as in PREM, because we do not want the amplitude curve to actually level off). We found that we could fit the North Pacific profile fairly well with the model PAC + (Fig. 7), which is identical with 690.B down to a depth of 150 km above the CMB, where the velocity gradient is decreased by 25%. This model is somewhat more complicated than the other two PAC models, but still represents a very simple way to model the data and thus is consistent, in principle, with the others. The slight decrease in gradient at the base of the mantle in the PAC + model is not particularly well resolved, but the overall faster velocity structure is: it is clear from the data profiles that the North Pacific region is faster than the Central Pacific and North Polar regions.

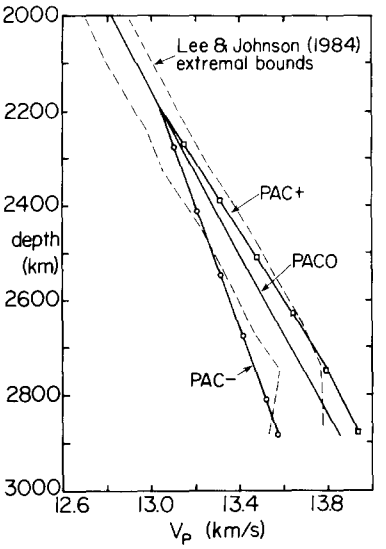

Fig. 8. A summary P-wave velocity versus depth plot showing all three PAC models and the extremal mantle velocity reference bounds determined by Lee and Johnson (1984). The bounds indicate a 97% confidence interval on a global set of travel time data.

5. Comparison with other data

We have proposed models for the lower mantle which deviate from an accepted reference Earth model (PREM) well above the traditional limit (the top of D″) for such deviations: are these models unreasonable? Figure 8 shows the three models along with extremal velocity bounds calculated for the lower mantle by Lee and Johnson (1984). These bounds indicate a 97% confidence interval on radial Earth models compatible with a set of global ISC travel times. These bounds do not indicate the 'correct' velocity profile in any given region, since they represent a global average; however, the width of the confidence interval grows only slightly with depth, which does not imply that any deviations from reference models should be limited to D″. Though we do not expect our models to be globally representative, the average of the three PAC models falls within the bounded region.

To assess the validity of the PAC models further, we compared the travel times predicted by the velocity models with the observed values. The three models certainly predict travel time differences, but the poor time resolution of the data owing to uncertainty in origin times, source depths, and receiver effects can make these differences difficult to detect. Figure 9a shows the travel time residual curves relative to the JB model (Jeffreys and Bullen, 1940) calculated by ray tracing for the PAC models. The data are shown in Fig. 9b–d. The baselines of the data are poorly resolved, but trends in the residuals with distance may still be diagnostic of structural variations. Linear regressions of the data are shown for distances beyond 78°, which is the distance where the PAC travel time curves are expected to diverge. The trends of the regressed lines agree qualitatively with the model behavior, but clearly the slopes are much less than predicted. It is unlikely that the travel time differences between PAC + and PAC0 or even between PAC − and PAC0 could be unambiguously detected without a more detailed study, but the differences between PAC + and PAC − , which are on the order of 5 s at the greatest separation of the travel time curves, should be resolvable even by our sparse set of travel time data. A comparison of Fig. 9a with

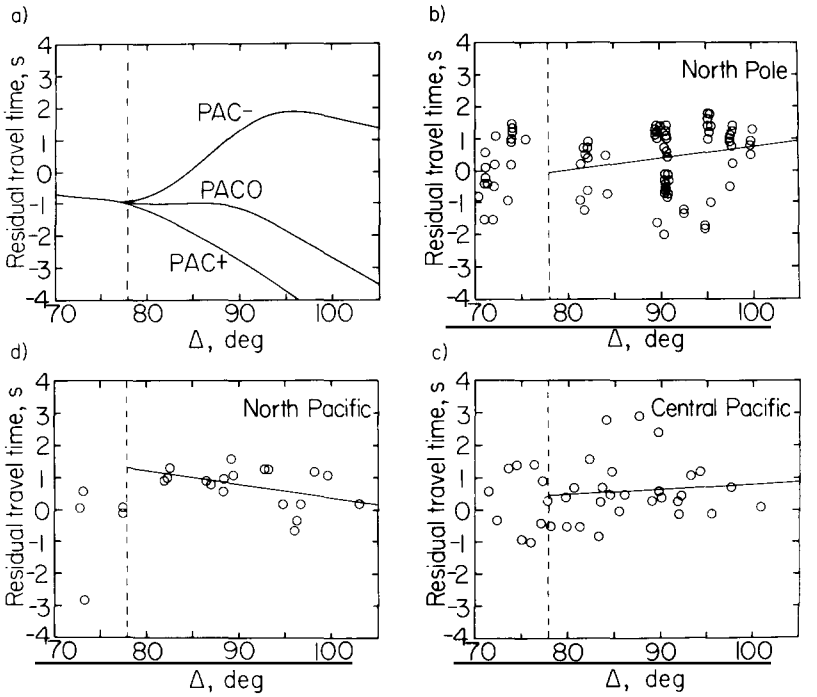

Fig. 9. A comparison of (a) the P-wave travel time JB residuals calculated for the PAC models with (b,c,d) JB data residuals from the same three source to North American WWSSN receiver combinations as for the amplitude data. The dashed lines indicate the distance (78°) beyond which the travel time curves for the PAC models diverge. Solid lines in the data plots are linear regression fits to the data to the right of the dashed lines. The travel time curves for the PAC models were calculated by ray-tracing and the JB times were then subtracted. The North and Central Pacific travel times were measured directly from the raw seismograms and JB times were then subtracted out. The North Pole JB residuals were taken (already measured and differenced) from the ISC bulletins. Station corrections (Dziewonski and Anderson, 1983) were applied to all of the data.

Fig. 9b and d indicates that the measured difference is smaller than predicted. While this result does seem to suggest that the PAC − and PAC + models are probably too extreme, the amount of overestimation is difficult to resolve. The relationship between velocity structure, travel times, and amplitudes in laterally varying structure is not well understood. According to Fig. 9a, the travel time differences between PAC − and PAC + should increase with distance, becoming largest at diffracted distances. However, raypaths to large distances have long path lengths in D″, perhaps too long to be characterized with our locally valid one-dimensional models. Thus it is reasonable that the travel time differences of diffracted waves may be smaller than expected. Nevertheless, in a more extensive global body-wave travel time study, Julian and Sengupta (1973) found relative velocity

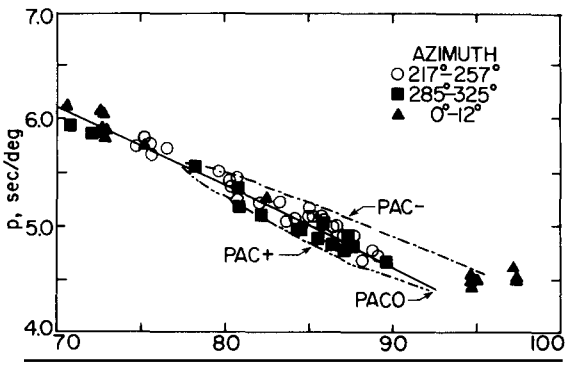

Fig. 10. Ray parameter versus distance for the PAC models and for SCARLET data from Burdick and Powell (1980). Additional data from 10 Soviet tests and a Soviet earthquake have been added. The data have been windowed into azimuthal ranges that sample the same general regions of D″ that we have modeled. Ideally, filled squares should correlate with PAC+, open circles with PACO, and filled triangles with PAC.

contrasts consistent with our models for nearly equivalent patches of the lower mantle.

Of course, absolute travel time information has always been difficult to obtain, and consequently many studies have measured slowness instead, because this can be done with good accuracy using arrays. We checked the PAC models against the Burdick and Powell (1980) slowness data set. Their data set consists of slowness measurements for 145 azimuthally distributed events detected by the SCARLET array in southern California, an array known to have particularly small mislocation vectors, indicating that receiver structure biases are effectively averaged out. We grouped the slowness measurements into azimuthal ranges that sample the same general patches of D″ which we modeled with the PAC models. The Burdick and Powell data set has only a few events from the azimuthal range corresponding to the North Polar patch of D″ (modeled with PAC −), so we supplemented it with SCARLET measurements of 10 Soviet tests and a Soviet earthquake. The grouped slowness measurements are plotted in Fig. 10 along with slowness curves calculated for the PAC models. Although there is significant scatter and the data are not uniformly distributed, there is a general correlation between the predicted model slownesses and the measured slownesses: PAC − has higher slowness values and PAC + has lower slowness values. Since the receivers and sources are not identical, we do not expect a perfect agreement, but the slowness observations alone suggest velocity structure variations comparable with those in the PAC models.

It is also possible to perform an analysis of amplitude data from arrays, and this has been done by Lay et al. (1979) for a set of Soviet nuclear tests recorded by the SCARLET array. They used a technique similar to that of Ruff and Helmberger (1982) to reduce the amplitude scatter in their data. The resulting profile (Fig. 11), which represents the same North Polar path through D″ as the Ruff and Helmberger data, is sensitive to a much smaller region owing to the limited size of the array, but clearly shows the same basic trend, and can also be fit by the PAC − model. Note that this profile is clearly inconsistent with the PAC0 and PAC + profiles, which have core

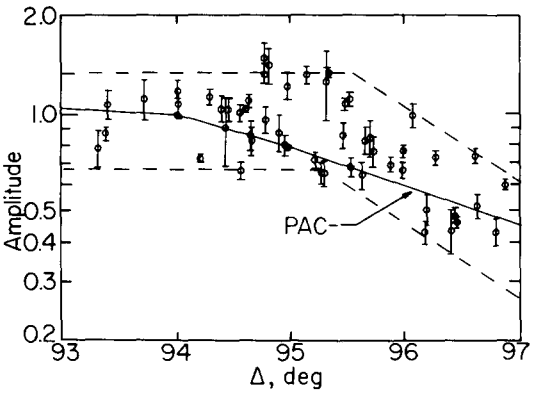

Fig. 11. A log amplitude versus distance plot of short-period P-wave data recorded by the SCARLET array for Soviet nuclear tests. The solid line is the profile for PAC − (Figure 6). The data are from Lay et al. (1979).

shadow onsets 5° closer. The fact that a consistent amplitude profile is shown by this data set is very significant: it indicates that the data profile in Fig. 6 is most strongly controlled by radial, not lateral, velocity contrasts, further supporting the validity of locally layered modeling. The rather high ray parameters (the points near 95° in Fig. 10) for the data in Fig. 11 are also very consistent with the PAC − model. Unfortunately, the distances of the other two source regions to the SCARLET array are not near the edges of the core shadow zones, so we could not make a similar array amplitude comparison for the two Pacific D″ regions.

6. Model resolution

While it is tempting to interpret our models in terms of global lower mantle structure as has been done in many other studies, we approach such interpretations with caution. In this study we have sampled only three small portions of the lower mantle. The three models can be confidently compared because they were derived in a consistent manner, but we still must recognize the limitations in the resolution of the data and in our modeling. The fact that we were able to match the observed profiles with such simple velocity structures probably says more about the resolution of our modeling technique than it does about the presence or

absence of fine-scale features in the lower mantle. The strongest conclusions which we can reach are that the velocities in the lowermost mantle beneath the Central Pacific are lower than those beneath the North Pacific but higher than those beneath the North Pole, and that, despite these gross velocity differences, positive P velocity gradients in D″ are required for all three regions.

In the modeling which led to the PAC models, we explicitly sought the 'simplest' models capable of explaining the data, basically exploring the model space with only one change in lower mantle velocity gradient. To minimize the required gradient change a thick zone of lateral variations was adopted, which extends 690 km above the core. The question arises as to whether such a thick zone is required, since the perturbations to a thinner zone would clearly reduce the predicted travel time anomalies. In order to evaluate this aspect of the PAC models, we calculated synthetics for two models, 350.A and 350.B, which have the same CMB velocities as 690.B (PAC + without the slight gradient reduction 150 km above the core) and 690.D (PAC −), but whose gradient change depths are located only half as far (350 km instead of 690 km) above the CMB. These models and their short-period P-wave amplitude profiles are shown in Fig. 12a. PAC0 is included for comparison.

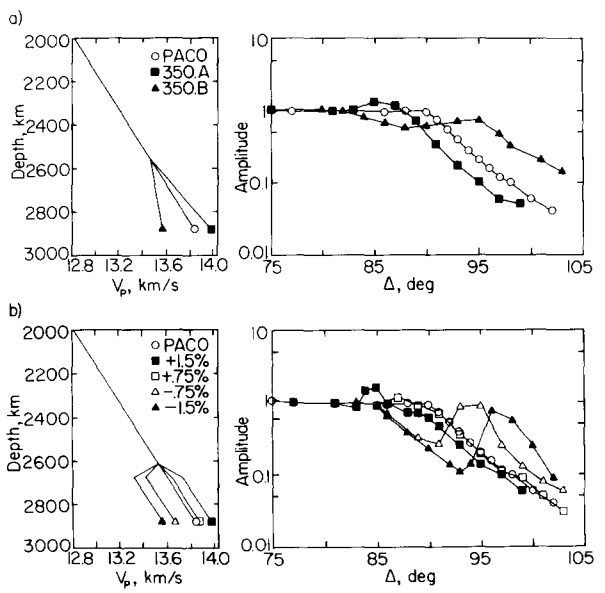

Fig. 12. Lower mantle P velocity structures and the resultant short-period amplitude versus distance profiles for: (a) PAC0 and two models which have velocity gradient changes 350 km above the CMB, and (b) PAC0 and four models whose velocities deviate from PAC0 280 km above the CMB by −0.75, −1.5, +0.75, and +1.5%.

The profiles for models 350.A and 690.B (Fig. 3a) have similar core shadow zone onset distances and decreasing amplitude slopes within the shadow zone, but differ in the distance range 83–88°. In this range, the 350.A amplitude profile displays a slight amplitude increase and subsequent decrease, while the 690.B profile has constant amplitudes out to the edge of the shadow zone. The amplitude fluctuation of the 350.A profile is caused by constructive interference of energy turning above and below the depth of the gradient change. The size of the increase near 85° is not consistent with the data in Fig. 7, hence we do not consider model 350.A to be a reasonable velocity structure for the lower mantle beneath the North Pacific. The 690.B profile does not have a similar feature because of the smaller gradient change for that model, and clearly provides a superior match to the data.

Comparison of the profiles for 350.B and 690.D (Fig. 3a) indicates a similar problem: again, the shadow zone onset distances and shadow zone amplitude decay slopes are similar, but the amplitudes at distances closer than the edge of the shadow zone are not. In this case, model 350.B has a slight amplitude dip over the range 81–95°, while the 690.D profile has constant amplitudes. The explanation for this sort of amplitude decrease has already been discussed: the decrease in velocity gradients spreads the wavefront out over a larger area, hence decreasing amplitudes. This dip in amplitude would match the lowest of the observed amplitudes near 90° in Fig. 6, but there are many observations at this distance which are not low relative to the data at 85°. Once again, the smaller gradient change of the 690 type model yields a smoother baseline which is more in keeping with the observed profile.

From these comparisons, we conclude that two of the characteristic features of our data sets, the distances of the onset of the core shadow zone and the amplitude decay slopes within the shadow

zones, can be matched equally well by positive gradient models which have deeper velocity gradient changes, but the third feature, approximately constant amplitudes at all distances closer than the onset of the core shadow, cannot be. In order to have sufficiently fast or slow average lowermost mantle regions with positive velocity gradients to match the first two features, the velocity gradient change must increase as the perturbed zone is narrowed. However, if the gradient changes are too strong, they will lead to violations of the constant amplitudes exhibited by the data for distances closer than the core shadow. Thus, while 690 km above the CMB is not a well-constrained depth, it is apparent that to fit the flat portions of the data amplitude profiles using simple, two velocity gradient models, the depth of gradient changes must be shallower than 350 km above the CMB. A reasonable minimum distance is probably 400 km. Of course, smoothly varying models can be used as well and no great significance should be attached to the precise depth at which the PAC models have changes in gradient.

More detailed velocity structures could not be uniquely resolved with this modeling scheme, but the viability of some of the more extreme velocity models proposed for the lower mantle can be evaluated. Within the last decade, several models have been proposed which have sharp velocity increases (Wright and Lyons, 1981; Lay and Helmberger, 1983) or decreases (Haddon and Buchbinder, 1987) in the lowermost mantle. To test the compatibility of these types of models with the short-period amplitude data, we calculated synthetics for the four models shown in Fig. 12b (again, PAC0 is included for comparison). These models are identical to PAC0 to a depth of 280 km above the CMB, at which depth the velocity for each increases or decreases by 0.75 or 1.5% over a distance of 60 km. Below this the PAC0 gradient continues to the CMB.

Let us begin with the most extreme model, the 1.5% decrease. The low-velocity zone leads to a large amplitude dip in the range 85–95°. This interval of decreased amplitudes is actually the shadow zone caused by the velocity decrease, and it is weakly illuminated by energy diffracted through the low-velocity channel. Interestingly, while the amplitude dip clearly disagrees with all of our data, the distance of the core shadow onset and the decay slope within it are fairly compatible with the North Polar data. Again, this is because these features are controlled by the average velocity structure at the base of the mantle (note that the −1.5% model is slow, as are the PAC − and POLAR models), and the velocity gradient just above the CMB (positive in each case). Thus, they can be fit by a model which has a single, reduced, positive velocity gradient, or by a model which has a strong negative velocity gradient followed by a strong positive gradient. It is the constant amplitude portion of the data profile which allows us clearly to choose the former type of model as superior.

The profile for the 0.75% decrease model is intermediate to the profiles for the 1.5% decrease model and PAC0, as one would expect. The size of the amplitude dip is smaller, and the edge of the shadow zone has moved closer to that of PAC0. However, the profile is still grossly incompatible with the three data profiles, suggesting that any sharp P velocity decrease in D″ must be very small, on the order of that in the POLAR models of Ruff and Helmberger (1982).

The velocity increase models provide more reasonable amplitude profiles (Fig. 12b), but this is not surprising because they do not represent such drastic modifications of PAC0. The PAC0 model increases velocity by 0.5% over a 60-km interval, so these models actually only represent 0.25 and 1.0% increases from PAC0. The distinctive feature of these profiles is the amplitude increase and subsequent decrease that each shows over a range of a few degrees at distances just closer than the onset of the core shadow. Clearly, the height of this feature is proportional to the size of the velocity increase: the amplitude augmentation for the 1.5% model is about twice as large as for the 0.75% model. The enhanced amplitudes are caused by the interference of energy from above and below the depth of the gradient change, as was discussed above for the 350.A model (Fig. 12a). Notice also that the distance of the onset of the shadow zone is closer for the faster +1.5% model than for the +0.75% model, as we would expect. While it would be difficult to say that the small

amplitude augmentation caused by the 0.75% increase is incompatible with the relatively constant amplitudes of the data at distances closer than the core shadow, the corresponding feature in the profile for the 1.5% increase model is probably too large. Hence, we conclude that an amplitude increase of more than about 1% spread out over a depth of 60 km or less in the lower mantle is not compatible with these data.

7. Discussion

This analysis indicates that there are strong lateral variations in the P velocity structure of D″ with scale lengths on the order of 1000 km. The variations extend at least 350 km above the CMB, and in at least three isolated regions the dominant P velocity gradient in D″ is positive. These strong variations are compatible with the longer wavelength variations inferred from global tomography (Dziewonski, 1984), and it is interesting to note that the D″ region near the North Pole is slower than average, while an adjacent region is fast. This strong gradient in D″ velocity structure at high latitudes may be responsible for the difficulty of resolving CMB topography and core anisotropy, since it is necessary to correct core phases for their mantle paths (e.g., Creager and Jordan, 1986; Morelli et al., 1986).

Our data set neither proves nor disproves the presence of boundary layers at the bottom of the mantle, but it does place some constraints on them. A thermal boundary layer in chemically homogeneous material is generally expected to be accompanied by a decreased velocity gradient (Doornbos and Mondt, 1979; Doornbos et al., 1986), although at high pressures the temperature derivative of seismic velocities may be much less than previously thought (Anderson, 1987). We found evidence for a decreased gradient in only one of the three regions we studied (discounting the slight decrease for the North Pacific region, which is not well resolved), suggesting that any global decrease in the velocity gradient at the bottom of the mantle may be relatively small. A pervasive negative velocity gradient in D″ is clearly inconsistent with these data. Ruff and Helmberger (1982) showed that a very thin region with a negative velocity gradient can be introduced just above the core, but it must be small enough to be masked by an overlying positive velocity gradient in D″. The data may be compatible with a chemical boundary layer, but only if the layer represents a gradual transition from the material above it, as far as P velocity is concerned: the amplitude profiles are too smooth to allow any large, discontinuous changes in material properties. Obviously, given the scatter in all three data sets, we cannot rule out sharp temperature or compositional contrasts on much smaller scales. These results are not inconsistent with previous S wave modeling: the one common region for which both types of data have been analyzed, the North Pacific, is believed to have fast S wave velocities in D″ as well (Lay and Helmberger, 1983). However, it does appear that the S wave velocity increase is stronger than the P velocity increase in this area, and that the S velocity gradients in D″ appear to be lower.

The great task now facing scientists who study the lowermost mantle is the reconciliation of the apparently contradictory evidence from the many different studies of the region. Increasingly, it seems that for such a reconciliation to be brought about, there must be a willingness on the part of researchers to question ideas about deep Earth structure which they have in the past treated as axiomatic. An emerging perspective of the base of the mantle which allows many of the seemingly conflicting observations to be reconciled is that of a combined chemical and thermal boundary layer, similar in some respects to the lithosphere. Lateral variations in P velocity and S velocity structure within D″ have many scale lengths, but, as we have shown in this study, it does appear that long wavelength variations are sufficiently strong to permit regional characterizations of discrete areas using locally stratified models. This can be interpreted as evidence for large-scale patches of compositional heterogeneity, perhaps akin to continents embedded within a dynamic thermal boundary layer (Jordan, 1979; Doornbos et al., 1986; Young and Lay, 1987a). A schematic diagram of this scenario is shown in Fig. 13. The basic attraction of this complex model is that it allows reconciliation of the evidence for strong

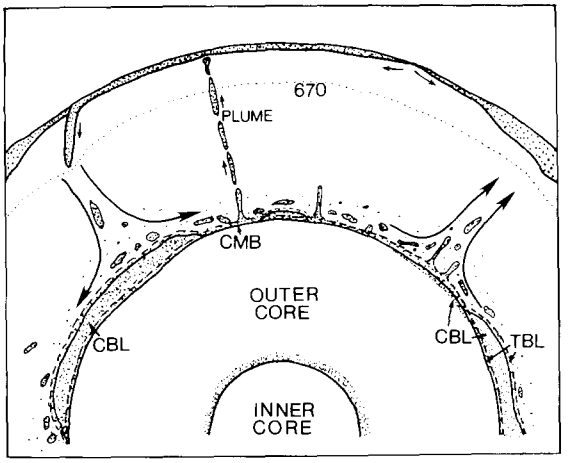

Fig. 13. A schematic diagram for the CMB region including the heterogeneity associated with both thermal boundary layer (TBL) and chemical boundary layer (CBL) structure. There may be some heterogeneity in the outermost core in regions of topographic highs on the CMB induced by large-scale upwelling in the mantle. Localized plumes due to thermal instabilities may also exist.

lateral heterogeneity with the evidence for locally coherent radial structure. Small-scale heterogeneity in the region may be the result of unsteady dynamics of the thermal boundary layer as well as localized compositional heterogeneity. The superadiabatic temperature gradient in the thermal boundary layer can provide part of the explanation for the greater reduction of S velocity gradients than P velocity gradients in D″. However, the temperature dependence of both seismic velocities is probably inhibited at high pressure (Anderson, 1987), so one must be cautious in interpreting temperature contrasts on the basis of the seismic models. Thermal effects alone cannot explain the evidence for S wave velocity stratification (Lay and Helmberger, 1983; Young and Lay, 1987a), nor is it clear how the enhanced thickness of the heterogeneous region at the base of the mantle can be produced thermally. Numerical calculations suggest that pressure dependence of lattice conductivity may account for some thickening of the D″ layer, with a smaller overall temperature drop across the boundary layer (Anderson, 1987; Zhang and Yuen, 1988).

8. Conclusions

The overall behavior of short-period P-wave amplitude profiles near the core shadow zone for three regions of the lowermost mantle can be fit by models with simple, positive velocity gradients in the lowermost mantle. The coherence of the observed profiles indicates that they are most sensitive to a scale of heterogeneity which is larger than the sampled regions, a condition which must be met to justify radial modeling. For our modeling, we chose to focus on matching three characteristic features of the observed profiles: the nearly constant amplitudes at distances closer than the shadow zone onset, the distance of that onset, and the amplitude decay slope within the shadow zone. We found that the latter two features are sensitive only to the average lower mantle velocity and the velocity gradient in D″, and so cannot be used to discriminate between models which are equivalent in terms of these parameters, but the former feature is incompatible with sharp gradient changes in D″, and so favors smoothly varying models. While our modeling technique lacks the resolution to test the validity of more complicated, multiple-gradient velocity structures which may be compatible with the data, we are able to show the incompatibility of sharp P velocity decreases or increases of greater than ~ 1%. The simplest class of models found to fit the observed profiles deviate from the PREM reference Earth model 690 km above the CMB, but show no obvious disagreement with mantle velocity bounds. Furthermore, theoretical slowness values calculated for them are consistent with observed values for the modeled regions. Models with significantly decreased velocity gradients 150 km or less above the CMB lead to flattening of amplitude versus distance curves well into the shadow zone which are not observed in any of the data sets. Our analysis indicates that the D″ velocities under the North Pole are ~ 2% slower than those under the Central Pacific, while the velocities under the North Pacific are ~ 1% faster, and that the lowermost mantle velocity gradient in each region is positive.

Acknowledgements

C.J.Y. was supported by an NSF Graduate Fellowship. We thank Larry Ruff for numerous discussions of the modeling procedure, and Bart Tichelaar for his helpful suggestions. Excellent criticism of the manuscript was provided by D.L. Anderson, Brian Cohee, Susan Schwartz, and Megan Wood. This research was supported by National Science Foundation Grant EAR-8451715, and by a Shell Faculty Career Initiation Grant to T. Lay.

References

Anderson, D.L., 1987. A seismic equation of state II. Shear properties and thermodynamics of the lower mantle. Phys. Earth Planet. Inter., 45: 307–323.

Burdick, L.J. and Powell, C., 1980. Apparent velocity measurements for the lower mantle from a wide aperture array. J. Geophys. Res., 85: 3845–3856.

Butler, R. and Ruff, L.J., 1980. Teleseismic short-period amplitudes; source and receiver variations. Bull. Seismol. Soc. Am., 70: 831–850.

Chapman, C.H. and Phinney, R.A., 1972. Diffracted seismic signals and their computational solution. In: B.A. Bolt (Editor), Methods in Computational Physics, Vol. 12, Academic Press, New York, pp. 165–230.

Creager, K.C. and Jordan, T.H., 1986. Aspherical structure of the core–mantle boundary from PKP travel times. Geophys. Res. Lett., 13: 1497–1500.

Doornbos, D.J., 1983. Present seismic evidence for a boundary layer at the base of the mantle. J. Geophys. Res., 88: 3498–3505.

Doornbos, D.J. and Vlaar, N.J., 1973. Regions of seismic wave scattering in the Earth's mantle and precursors to PKP. Nature, 243: 58–61.

Doornbos, D.J. and Mondt, J.C., 1979. P and S waves diffracted around the core and the velocity structure at the base of the mantle. Geophys. J. R. Astron. Soc., 57: 181–195.

Doornbos, D.J., Spiliopoulos, S. and Stacey, F.D., 1986. Seismological properties of D″ and the structure of a thermal boundary layer. Phys. Earth Planet. Inter., 41: 225–239.

Dziewonski, A.M., 1984. Mapping the lower mantle: determination of lateral heterogeneity in P velocity up to degree and order 6. J. Geophys. Res., 98: 5929–5952.

Dziewonski, A.M. and Anderson, D.L., 1981. Preliminary reference Earth model. Phys. Earth Planet. Inter., 25: 297–356.

Dziewonski, A.M. and Anderson, D.L., 1983. Travel times and station corrections for P-waves at teleseismic distances. J. Geophys. Res., 88: 3295–3314.

Haddon, R.A.W., 1982. Evidence for inhomogeneities near the core–mantle boundary. Phil. Trans. R. Soc. London, Ser. A, 306: 61–70.

Haddon, R.A.W. and Buchbinder, G.G.R., 1987. S wave scattering by 3-D heterogeneities at the base of the mantle. Geophys. Res. Lett., 14: 891–894.

Helmberger, D.V., 1974. Generalized ray theory of shear dislocations. Bull. Seismol. Soc. Am., 64: 45–64.

Hofmann, A.W. and White, W.M., 1982. Mantle plumes from ancient oceanic crust. Earth Planet. Sci. Lett., 57: 421–436.

Jeanloz, R. and Richter, F.M., 1979. Convection, composition, and the thermal state of the lower mantle. J. Geophys. Res., 84: 5497–5504.

Jeffreys, H. and Bullen, K.E., 1940. Seismological Tables. British Association for the Advancement of Science, Gray–Milne Trust, London, 55 pp.

Jordan, T.H., 1979. Structural geology of the Earth's interior. Proc. Natl. Acad. Sci. U.S.A., 1976: 4192–4200.

Julian, B.R. and Sengupta, M.K., 1973. Seismic travel time evidence for lateral inhomogeneity in the deep mantle. Nature, 242: 443–447.

Lay, T. and Helmberger, D.V., 1983. A lower mantle S-wave triplication and the shear velocity structure of D″. Geophys. J. R. Astron. Soc., 75: 799–833.

Lay, T., Minster, B. and Ruff, L.J., 1979. Application of the Southern California Array to teleseismic studies. EOS, 60: 880.

Lee, R.C. and Johnson, L.R., 1984. Extremal bounds on the seismic velocities in the Earth's mantle. Geophys. J. R. Astron. Soc., 77: 667–681.

Loper, D.E. and Stacey, F.D., 1983. The dynamical and thermal structure of deep mantle plumes. Phys. Earth Planet. Inter., 33: 304–317.

Morelli, A., Dziewonski, A.M. and Woodhouse, J.H., 1986. Anisotropy of the inner core inferred from PKIKP travel times. Geophys. Res. Lett., 13: 1545–1548.

Mula, A.H. and Müller, G., 1980. Ray parameters of diffracted long period P and S waves and the velocities at the base of the mantle. Pure Appl. Geophys., 118: 1272–1292.

Ruff, L.J. and Anderson, D.L., 1980. Core formation, evolution and convection: a geophysical model. Phys. Earth Planet. Inter., 21: 181–201.

Ruff, L.J. and Helmberger, D.V., 1982. The structure of the lowermost mantle determined by short-period P-wave amplitudes. Geophys. J. R. Astron. Soc., 68: 95–119.

Ruff, L.J. and Lettvin, E., 1984. Short period P-wave amplitudes and variability of the core shadow zone boundary. EOS, Trans. Am. Geophys. Union, 65: 999.

Sacks, I.S., Snoke, J.A. and Beach, L., 1979. Lateral heterogeneity at the base of the mantle revealed by observations of amplitudes of PKP phases. Geophys. J. R. Astron. Soc., 59: 379–387.

Stacey, F.D. and Loper, D.E., 1983. The thermal boundary-layer interpretation of D″ and its role as a plume source. Phys. Earth Planet. Inter., 33: 45–55.

Woodhouse, J.H., Dziewonski, A.M., Giardini, D., Li, X.D. and Morelli, A., 1987. The emerging three dimensional structure of the Earth: results from the modelling of wave-

forms, free oscillation spectra and seismic travel times. EOS, Trans. Am. Geophys. Union, 68: 356.

Wright, C. and Lyons, J.A., 1981. Further evidence for radial velocity anomalies in the lower mantle. Pure Appl. Geophys., 119: 137–162.

Young, C.J. and Lay, T., 1987a. Evidence for a shear velocity discontinuity in the lower mantle beneath India and the Indian Ocean. Phys. Earth Planet. Inter., 49: 37–53.

Young, C.J. and Lay, T., 1987b. The core–mantle boundary. Ann. Rev. Earth Planet. Sci., 15: 25–46.

Zhang, S. and Yuen, D.A., 1988. Dynamical effects on the core–mantle boundary from depth-dependent thermodynamical properties of the lower mantle. Geophys. Res. Lett., 15: 451–454.